



ARTICLE

Preparation and Performance of Ternesite-Ye'Elimite Clinker Produced from Steel Slag at Lower Temperature

Zhengyang Li¹, Wei Guo^{1,*}, Yueyang Hu¹, Xiao Wang¹, Binbin Qian² and Cuifeng Jiang¹

¹Materials Science & Engineering, Yancheng Institute of Technology, Yancheng, 224001, China

²Department of Chemical Engineering, Monash University, Melbourne, 3800, Australia

*Corresponding Author: Wei Guo. Email: guowei68550@163.com

Received: 22 September 2021 Accepted: 08 December 2021

ABSTRACT

Ternesite ($4\text{CaO}\cdot 2\text{SiO}_2\cdot \text{CaSO}_4$)-Ye'elimite ($3\text{CaO}\cdot 3\text{Al}_2\text{O}_3\cdot \text{CaSO}_4$) (simplified as TY) cement clinker was successfully prepared from steel slag at 1200°C in this study. XRD, TG/DSC and SEM were used to analyze the mineral composition and hydration products of the TY clinker. The sintering process and hydration mechanism of the TY clinker were investigated. Results show that a large amount of ternesite and ye'elimite have been formed at 1200°C , while ternesite has not been decomposed. Clinker minerals include ternesite, ye'elimite, gypsum and a small amount of iron phase. Iron phase from steel slag can promote the formation of liquid phase with the presence of gypsum at 1200°C and thus lead to the coexistence of ternesite and ye'elimite. The compressive strength of TY cement cured at 28 d is 59.5 MPa, which is higher than that of P. II 42.5 cement. This research provides a sustainable and energy-effective way for the reutilization of steel slag, an otherwise valueless waste.

KEYWORDS

Liquid phase; low temperature calcination; steel slag; ternesite; waste utilization; ye'elimite

1 Introduction

Steel slag, a typical large-scale industrial solid waste, has a very low comprehensive utilization rate at present. The large amount of discharged steel slag not only occupies farmland, but also causes serious pollution to soil, groundwater and the air [1–3]. Thus, it has become an important issue which hinders the sustainable development of steel industry. Currently, there are a variety of methods for steel slag utilization, including direct paving materials, or a mixed material for steel slag cement production. However, it is still very difficult to solve the problem of volume instability for steel slag [4]. To eliminate the effect of instability, some researchers used it as a raw material to prepare cement clinker [5]. Studies have shown that when using steel slag in the cement production, the resultant clinker required a lower requirement for water to achieve standard consistency and delayed setting time. In addition, compressive strength of steel slag cement clinker is close to the ordinary cement clinker [6]. Therefore, steel slag can be used as a high-quality raw material in a kiln feed during cement production [7].

It is well established that ye'elimite ($3\text{CaO}\cdot 3\text{Al}_2\text{O}_3\cdot \text{CaSO}_4$) is a mineral possessing excellent properties including rapid hydration, high early strength, frost resistance and durability. Its sintering temperature is between 1250 and 1350°C [8,9]. While ternesite ($4\text{CaO}\cdot 2\text{SiO}_2\cdot \text{CaSO}_4$) has long been considered as a



hydrating inert mineral. It can be produced at the temperature range of 1050–1200°C while decomposed above 1250°C [10–16]. Recent studies [9] have shown that aluminum hydroxide ions generated during the hydration of ye'elimite have a significant excitation effect on the hydration of Ternesite and ternesite releases gypsum during the hydration process, which further promotes the formation and stability of ettringite. Since Heidelberg cement company produced BCT (Beilite-Calcium sulphoaluminate-Ternesite) cement clinker at 1250–1350°C [17], the preparation of clinker containing ternesite has become a research hotspot of alite-ye'elimite cement. Shen et al. [9] obtained ternesite-belite-calcium sulphoaluminate cement by using bauxite and limestone as raw materials for first thermal insulation at 1270°C for 30 min and then calcined again at 1100–1200°C for 2 h. Commonwealth Scientific and Industrial Research Organisation [18–20] took fly ash and other industrial waste as the main raw materials and adopted a three-stage sintering process of thermal insulation at 1200°C for 8 h, then at 850°C for 2 h and finally at 1000°C for 1 h to prepare clinkers containing ternesite and ye'elimite. The calcining temperature of the clinker containing ternesite can be reduced by the multi-stage calcining process, however, the calcining system is complicated and time-consuming.

Considering that iron phase and trace elements in steel slag can promote the sintering of cement clinker, steel slag is hence used as a raw material to increase the amount of liquid phase and decrease the formation temperature of ye'elimite [21,22]. Timashev [23] found that the existence of iron can reduce the melt viscosity and surface tension of cement clinker, thus decreasing the temperature of liquid phase formation, increasing the crystallization rate of minerals, and promoting the formation of mineral phases, which is similar to the effect of the mineralizer. Another study [24] showed that a small amount of iron phase was conducive to reducing liquid phase viscosity under lower temperature conditions, facilitating solid phase reaction and promoting the formation of ye'elimite. Huang et al. [25] concluded that Fe_2O_3 can promote the absorption of free calcium oxide (f-CaO) in the clinker, increase the liquid phase, improve the flammability of mineral raw material and replace the Al^{3+} in Fe^{3+} to form solid solution $\text{C}_4(\text{A}_{0.95}\text{F}_{0.05})_6\text{O}_{12}(\text{SO}_4)$. Hu [26] reported that in the alite-ye'elimite cement clinker system, more ye'elimite was formed at lower temperature (1250°C) with the increase of iron content in the raw materials. A small amount of sulfur can improve the melting performance of the burned liquid phase and can react with $2\text{CaO}\cdot\text{SiO}_2$, which is favorable for the formation of ye'elimite and ternesite and plays a positive role in the production of cement clinker [27,28].

Herein, the preparation and performance of TY cement clinker prepared at 1200°C were investigated for the utilization of steel slag. In addition, the detailed sintering process and subsequent hydration mechanism of the as-prepared TY cement clinker were studied. Finally, the compressive strength was also tested to evaluate its mechanic performance. This study provides a sustainable and effective way for the utilization of steel slag and offers a new thought for the preparation of cement.

2 Experiment

The raw materials used in the experiment were steel slag, gypsum (99.5%), aluminum hydroxide (99.5%), calcium oxide (99.5%). The chemical composition of steel slag and OPC are shown in Table 1. XRD image of steel slag are shown in Fig. 1.

The bulk steel slag was crushed into small pieces by the jaw crusher, and then pulverized in the ball mill. The particle size distribution of the steel slag used in this research is shown in Fig. 2.

According to the alkalinity coefficient (C), Al/S ratio (P) and Al/Si ratio (N), the ratio design is $C \approx 1$, $P \leq 3.84$, $N \approx 2.55$. The raw materials were mixed according to Table 2. The mixtures were burned in an electric furnace at 1200°C for 2–4 h. Then the products were removed from the furnace and cooled rapidly in air with electric fan.

Table 1: Chemical composition of steel slag and OPC clinker (wt%)

Mineral	Steel slag	OPC
CaO	39.7	61.4
SiO ₂	19.8	21.5
Al ₂ O ₃	6.0	5.9
SO ₃	0.3	2.4
Fe ₂ O ₃	23.2	2.9
MgO	3.5	2.4
MnO	5.0	–
P ₂ O ₅	0.7	–
Ti ₂ O	–	2.4
k ₂ O	–	0.5
LOI	0.3	0.6

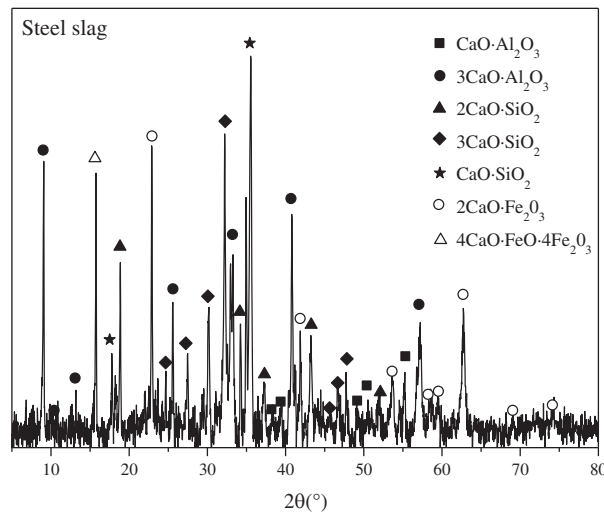


Figure 1: XRD diagram of steel slag

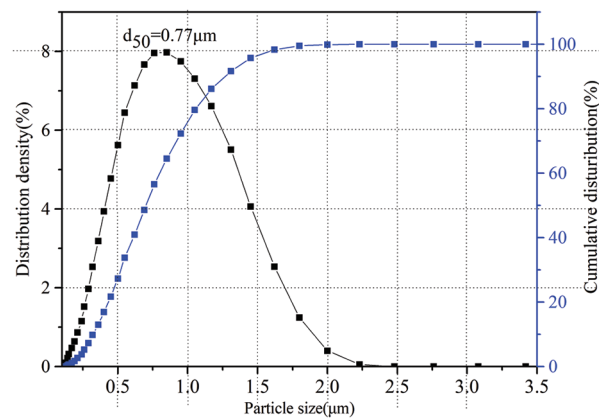


Figure 2: Particle distribution of steel slag size

Table 2: The mixture ratios of the raw materials (wt%)

Steel slag	CaO	Al(OH) ₃	CaSO ₄ ·2H ₂ O
67.67	8.52	17.44	21.35

The mineral phases of clinker produced by different calcining procedures were measured by using an X-ray diffractometer (X'Pert ProMPD PANalytical produced from PANalytical B.V. in Almelo, the Netherlands) with Cu-K α radiation, scanning at a range of 5–70° with a rate of 5°/min. Use external standard methods for detection [29,30].

Thermal analysis (TG-DTA) was performed on the samples in N₂ with Netzsch Sta449C thermal analyzer from NETZSCH Scientific Instruments Trading (Shanghai), Ltd. (China). The heating rate was 10 °C/min, rising from 20 to 1150°C.

The clinker minerals were analyzed by Nova NanoSEM 450 scanning electron microscope from FEI company, USA.

The Blaine surface areas of TY cement and OPC were $376 \pm 2.2\%$ and $354 \pm 3\%$ m²/kg, respectively. Cement paste with water to binder ratio of 0.45 was cast into steel mold of 20 mm * 20 mm * 20 mm. The compressive strength measurements were conducted at the curing age (3 d, 7 d, 14 d and 28 d).

To analyze the hydration process, A 3114/3236 TAM 83 Air (Thermometric AB) isothermal calorimeter equipped with an internal mixing device was used to determine the rate of hydration heat liberation. The pastes were formulated via the internal mixing procedure by 0.45 ml of water while every 1.000 g of mixed raw materials at 20°C. For the instrument to achieve thermal equilibrium, began to record the experiment data.

To investigate the hydration of TY cement and OPC, cement pastes were prepared with water/cement ratios of 0.45. All hydration experiments were carried out at 20°C.

At the end of different curing ages, the samples were crushed, treated with ethanol to stop hydration and stored in a desiccator. These samples were analyzed by XRD, SEM and TG-DTA [31–33].

3 Results and Discussion

3.1 Synthesis of TY Cement Clinker

3.1.1 XRD and TG-DTA

To investigate the reaction process, the raw materials were calcined at different temperatures (800, 900, 1000, 1100, 1150, 1200 and 1250°C) for 2 h. The XRD patterns are shown in Fig. 3. In order to analyze the influence of sintering process, the raw materials were also calcined at 1200°C for different times and the XRD patterns are shown in Fig. 4.

A large amount of 2CaO·SiO₂ and anhydrite were produced in the sample at 800°C (In Fig. 3). At 900°C, anhydrite and 2CaO·SiO₂ gradually decreased, while a small amount of ternesite and ye'elimite began to appear. With the increase of temperature, higher content of ternesite was produced. At 1000°C, ternesite was generated in large quantities and the anhydrite continued to decrease. ye'elimite began to generate at 1000°C. Meanwhile, CaO·Al₂O₃ and a small amount of ferrite phase also appeared. As the temperature went up, the diffraction peak of ye'elimite continued to increase, but no significant change for the diffraction peak of ternesite. When the temperature reached 1250°C, the diffraction peak intensity of anhydrite increased and ternesite decreased. Ternesite is a phase formed at the temperature range of 900–1200°C [21], while at the temperature higher than 1200°C, ternesite is decomposed into 2CaO·SiO₂ and anhydrite. Therefore, it is proposed that 1200°C is an optimal temperature for calcination of TY clinker. In Fig. 4, the main minerals in the calcined samples at 1200°C are ye'elimite, ternesite, a small

amount of anhydrite and ferrite phase. With the extension of the sintering time, the intensity of mineral diffraction peak of ternesite decreased, indicating that minerals continued to decompose with the extension of the sintering time. Therefore, TY cement clinker can be prepared at 1200°C, and prolonged sintering time is not favorable to the formation of ternesite.

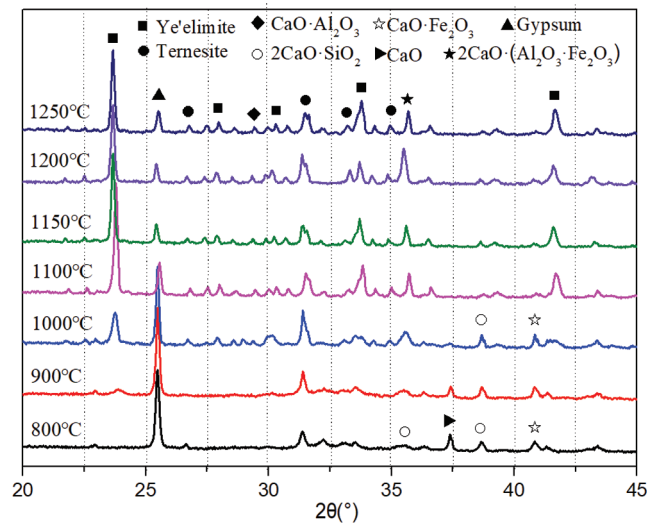


Figure 3: XRD patterns of samples at different temperatures

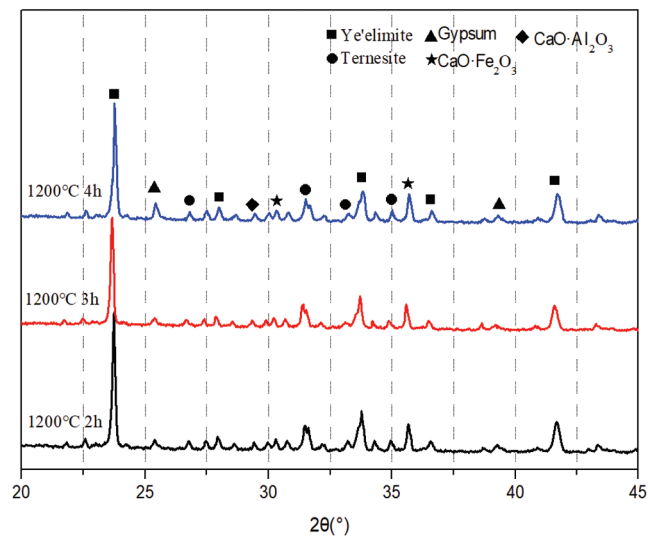


Figure 4: XRD patterns of samples with different holding time at 1200°C

The TG-DTA curve of raw materials heated from 20 to 1150°C is shown in Fig. 5. As can be seen from Fig. 5, the heat absorption peak at 120°C corresponds to the dehydration of dihydrate gypsum, and formation of hemihydrate gypsum. The heat absorption peak at 269°C and 369°C corresponds to the dehydration of $\text{Al}(\text{OH})_3$ and the further dehydration of hemihydrate gypsum to form anhydrite, respectively. The mass loss before 400°C is mainly caused by dehydration in the raw material. The absorption peak around 898°C was attributed to the formation of large amount of ye'elimite. The mass loss was very small in the

interval from 950 to 1100°C according to the TG curve, indicating that a large amount of ternesite and ye'elimite were formed in this interval which can be also verified from the XRD patterns in Fig. 4. The mechanism for the description of crystal phase conversion is shown in Fig. 6.

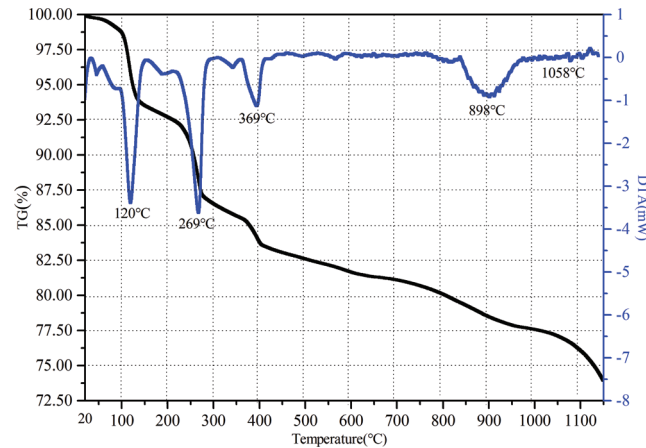


Figure 5: TG-DTA curve of the formation process of TY cement clinker

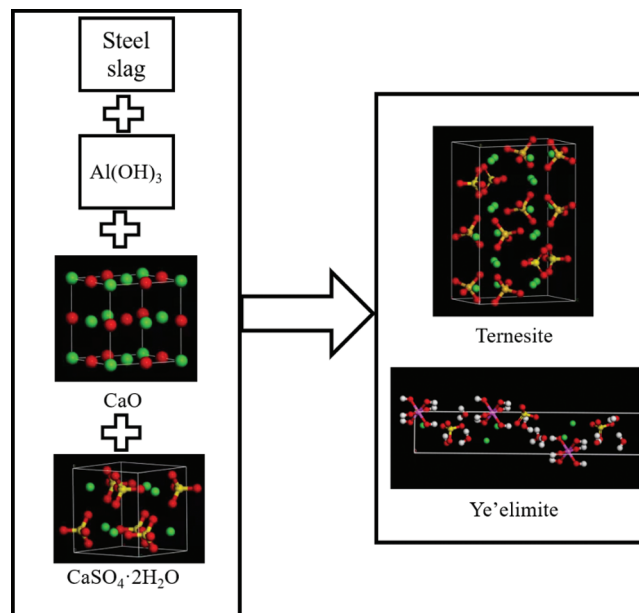
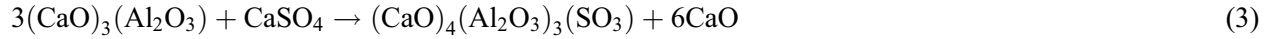


Figure 6: Mechanism of crystal phase conversion

From 900°C, ye'elimite and ternesite phase began to form, the equation is as follows (Eqs. (1)–(3)) [20,21]:





It is reported that $3\text{CaO}\cdot\text{Al}_2\text{O}_3$ reacted with anhydrite to form a small amount of ye'elimite when the temperature reaches 1250°C [32]. According to the XRD, $3\text{CaO}\cdot\text{Al}_2\text{O}_3$ in the raw material gradually disappeared with the increase of holding temperature [34].

3.1.2 SEM Analysis

Fig. 7a shows the microstructure of TY cement clinker produced at 1200°C for 2 h. Unlike Portland cement clinker, two different crystal morphologies are exhibited in this TY cement clinker. The microstructure of TY cement clinker confirms the existence of rod-shaped particles surrounded by many roundness particles. According to the analysis in Fig. 7b, the minerals of TY cement clinker were investigated. It can be determined that the rod-shaped particles are ternesite based on the element analysis. This is similar to the mineral TY cement clinker synthesized by Shen through secondary calcination [24]. There are a large number of small particles around $0.5\text{--}1\ \mu\text{m}$ in the clinker. According to the EDS it can be obtained that the roundness particles are ye'elimite. Compared with samples produced by different holding time, it was found that the amount of ternesite decreased obviously. This result is consistent with XRD analysis.

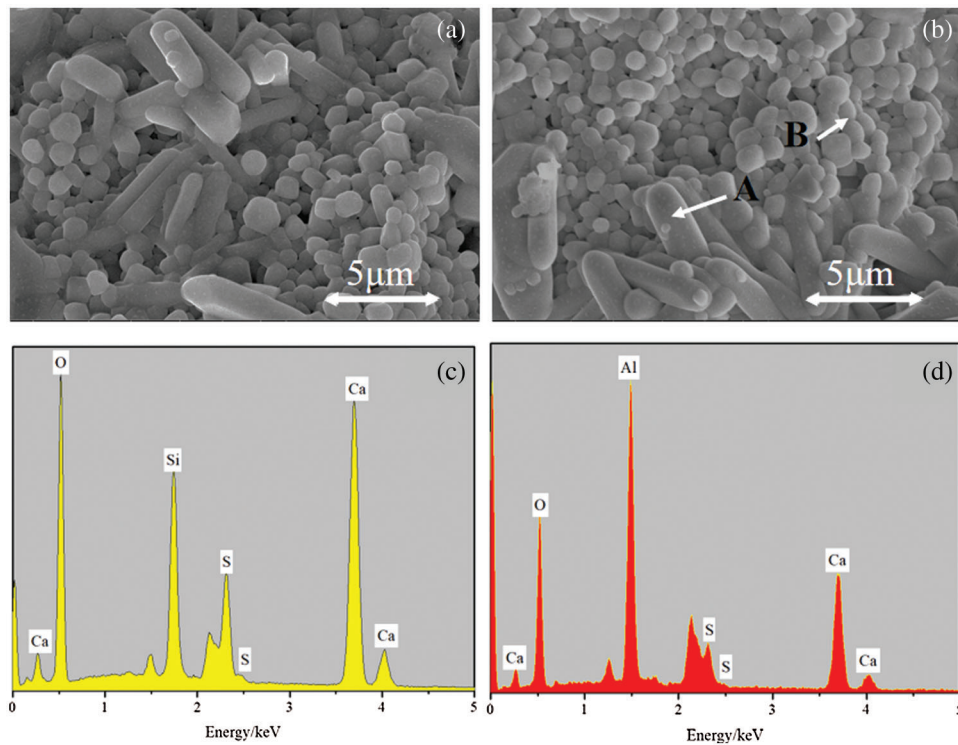


Figure 7: SEM and EDS of TY cement clinker at 1200°C for different time (a) and (b) for clinker calcined at 1200°C for 2 h; (c) and (d) for EDS analysis of point A and B in (b), respectively

3.1.3 Formation Mechanism of TY Cement Clinker

To investigate the composition of phases in the clinker, X-ray powder diffraction (XRD) analysis was used for phase identification and quantification. In this study, the external standard approach was used to obtain an absolute quantification of the crystalline-phase content.

The mass attenuation coefficients of the samples were independently determined by X-ray fluorescence analysis, as shown in Table 3. Each mineral content was calculated according to the Eq. (4), where S_{α} is the Rietveld scale factor of the mineral, ρ_{α} is the density of the mineral, V_{α} is the unit-cell volume of the mineral, μ_s is the sample mass absorption coefficient (MAC), G is the diffractometer constant, and W_{α} is the weight fraction of the mineral (Eq. (1)) [35]. The calculated results were provided in Table 4. XRD quantitative analysis was performed with Highscore Plus, as shown in Fig. 3.

$$W_{\alpha} = S_{\alpha} \frac{\rho_{\alpha} V_{\alpha}^2 \mu_s}{G} \quad (4)$$

Table 3: Chemical analysis and phase composition of TY cement clinker

Chemical composition	Content (g/100 g)	μ_m (cm ² /g)
CaO	40.47	124.04
Al ₂ O ₃	29.57	31.69
SO ₃	12.08	44.46
Fe ₂ O ₃	8.73	214.9
SiO ₂	4.41	36.03
MgO	2.48	28.60
P ₂ O ₅	0.51	39.66
TiO ₂	0.17	124.60
Na ₂ O	0.13	24.97

Table 4: Calculated the mineral content of TY cement clinker

Phase composition	ICSD code	G-factor (*10 ⁻⁴⁴ .cm ⁻⁵ /wt%)	Mineral content (wt%)
ye'elimitite	80361 [36]	3.69	47.1
Ternesite	4332 [37]		20.2
C ₂ (F _{1.4} A _{0.6})O ₈	2841 [38]		4.9
CaSO ₄	16382 [39]		5.4
ACn			22.4

In the clinker sintering process, the formation of the liquid phase plays a crucial role in both the rate and quality of clinker. It can be seen from Fig. 8 that at 1200°C, the main minerals in cement clinker are ye'elimitite, ternesite and a small amount of 2CaO·(Fe₂O₃·Al₂O₃). Meanwhile, up to 22.4% amorphous phase has also appeared. The content of amorphous phase is similar to that of Belite-calcium sulphoaluminate cement [40]. At 1200°C, a small amount of iron phase (C₂(F_{1.4}A_{0.6})O₈) in steel slag formed 2CaO·(Fe₂O₃·Al₂O₃) and 3CaO·3(Al₂O₃·Fe₂O₃)·CaSO₄. More iron phase had dissolved into the liquid phase, and promoted the formation of ye'elimitite. At this temperature, an hydrite is no longer visible, and most sulfur enters the clinker. In the process of burning sulphoaluminate cement, sulfur also plays a key role. On the one hand, sulfur can reduce the viscosity of liquid phase during the formation of clinker, which is conducive to the formation of ye'elimitite [9]. Moreover, it can form ternesite with 2CaO·SiO₂ at lower temperature.

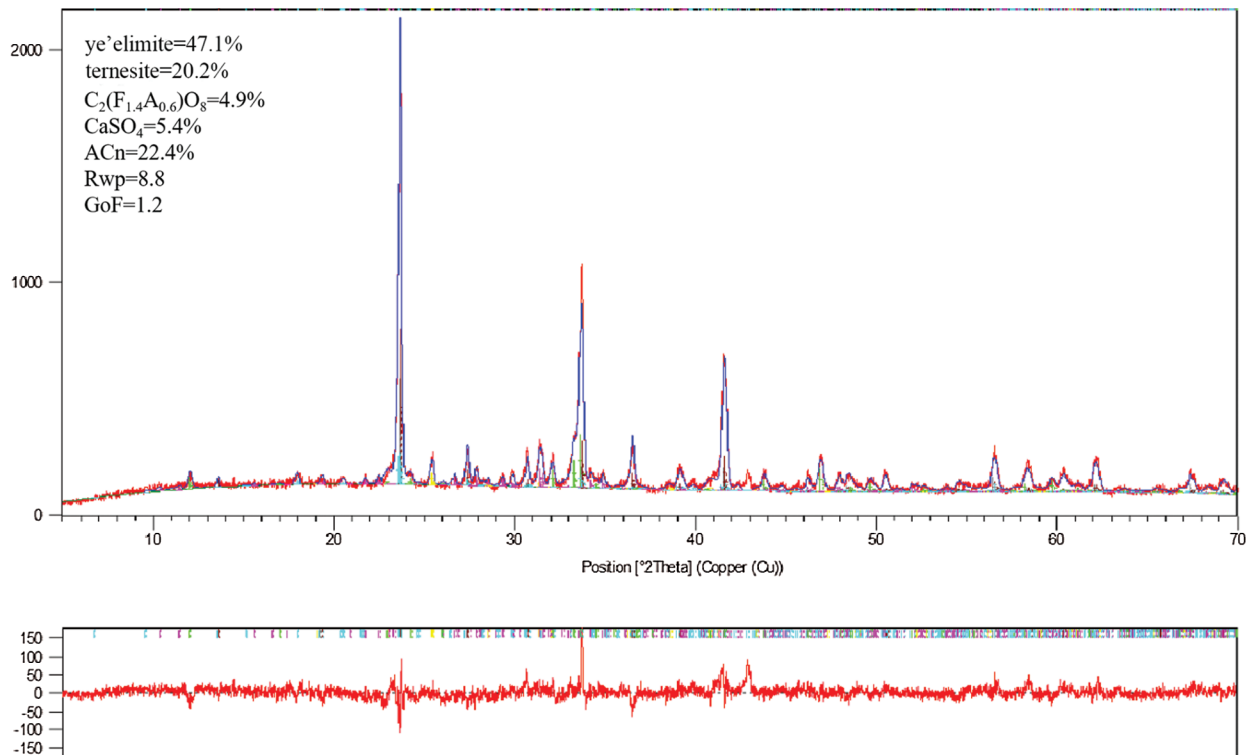


Figure 8: Rietveld refinement of the clinker produced at 1200°C for 2 h

In conclusion, the iron phase in steel slag can promote the formation of the liquid phase, which further leads to the coexistence ternesite and ye'elimite at 1200°C. TY cement clinker can be obtained in one step by calcining at 1200°C, which is 100°C lower than the traditional one-step method.

3.2 Hydration

3.2.1 Isothermal Calorimetry

The hydration exothermic-time curve of OPC and TY cement is shown in Fig. 9a. As can be seen, Peak 1 is the dissolution and the hydration of ye'elimite, Peak 2 is attributed to the dissolution of OPC and the hydration of $3\text{CaO}\cdot\text{Al}_2\text{O}_3$. The hydration rate of TY cement is higher within 0–35 min, reaching a maximum of 125 mW/g. Then, it entered the hydration induction period after 35 mins. The Peak 3 of OPC appeared at about 15 h, it normally corresponds to the alite hydration. Peak 4 is generally believed to be caused by the conversion of ettringite to AFm. Peak 5 is the reaction of ternesite.

It can be seen from Fig. 9b that the rate of heat release from hydration is very high in the early stage of both the two clinkers, and the cumulative heat release from hydration of TY clinker is higher in 0–35 min. After 35 min, OPC clinker occupies the dominant position. 5–30 h is the hydration acceleration period of OPC clinker, and the cumulative hydration heat release increases rapidly. During the hydration period between 25–50 h, the cumulative heat release increased sharply due to the secondary heat release of TY clinker, while the total heat evolved of hydration was lower than that of OPC clinker. The results show that the hydration of ternesite improved the strength of TY cement in the early and middle stage.

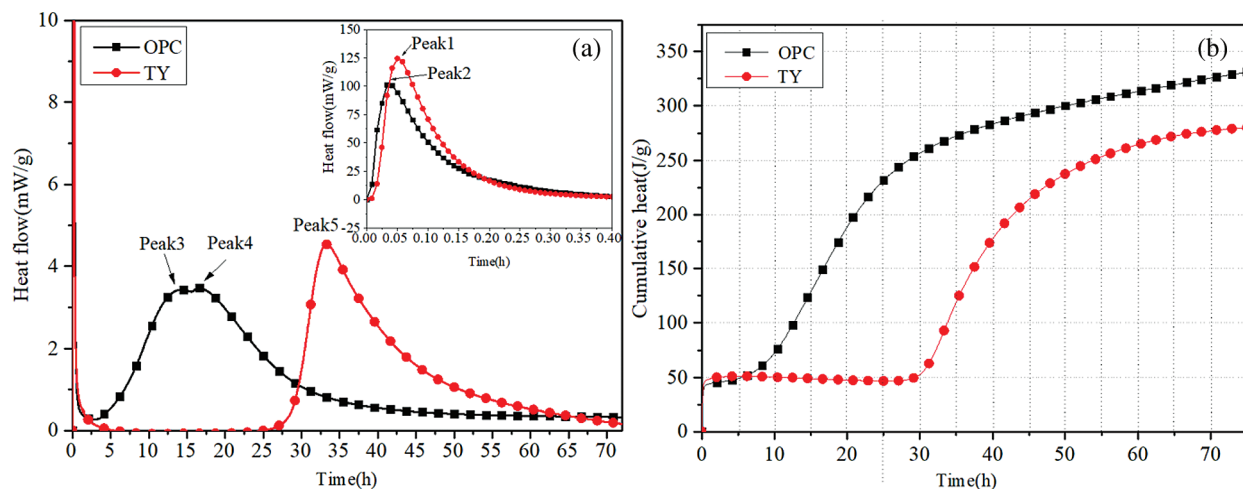


Figure 9: Hydration heat release (a) and cumulative hydration heat release (b) curve of OPC and TY cement

3.2.2 Hydrates

Hydrates of OPC and TY cement at different ages were measured by XRD, as shown in Fig. 10.

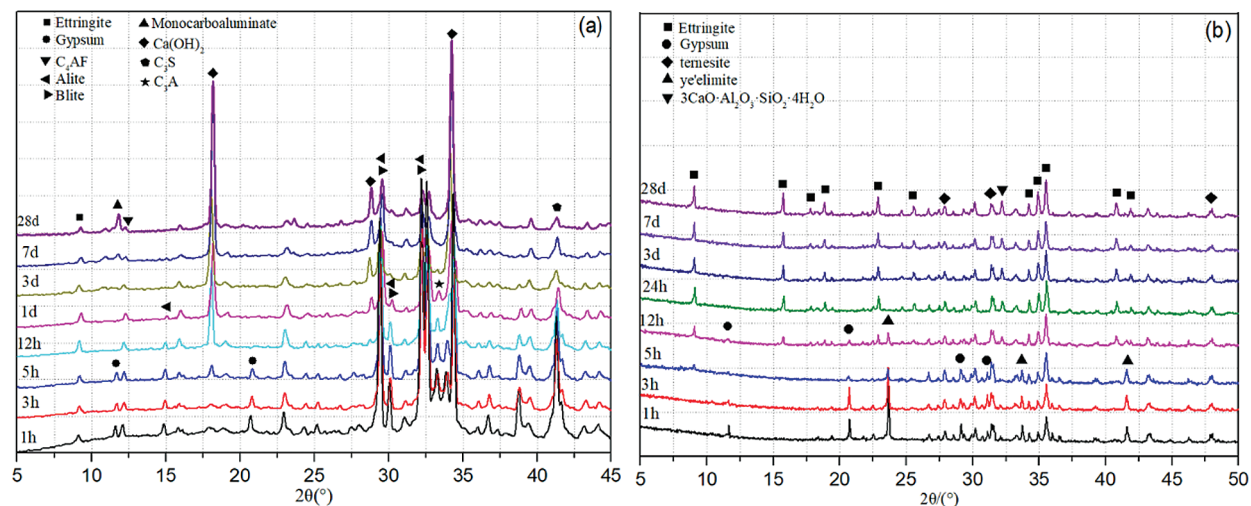


Figure 10: XRD patterns of hydrates of OPC (a) and TY cement (b) at different curing ages

The thermogravimetry curves of TY cement and OPC hydrates were measured from room temperature to 850°C, as shown in Fig. 11.

In OPC system, ettringite and Portlandite are the main crystalline products found by XRD and TGA at early ages. At 1 h, Aft was already formed. Gypsum disappeared within 1 d after hydration. Before 12 h, the amount of Portlandite was relatively low, while at 12 h, the amount of Portlandite began to increase rapidly. Because of the presence of CaCO₃, monocarboaluminate was found at 28 d. In the patterns of TGA, the weight losses from 50 to 110°C, 110–140°C, 140–160°C and 400–450°C indicate the loss of Aft, gypsum, AFm(CO₃) and Portlandite. Ettringite peaks were detected in the XRD and TGA patterns within a few hours and increased in intensity to a maximum. With no added gypsum, the ettringite evolved to the AFm phase (monosulfoaluminate).

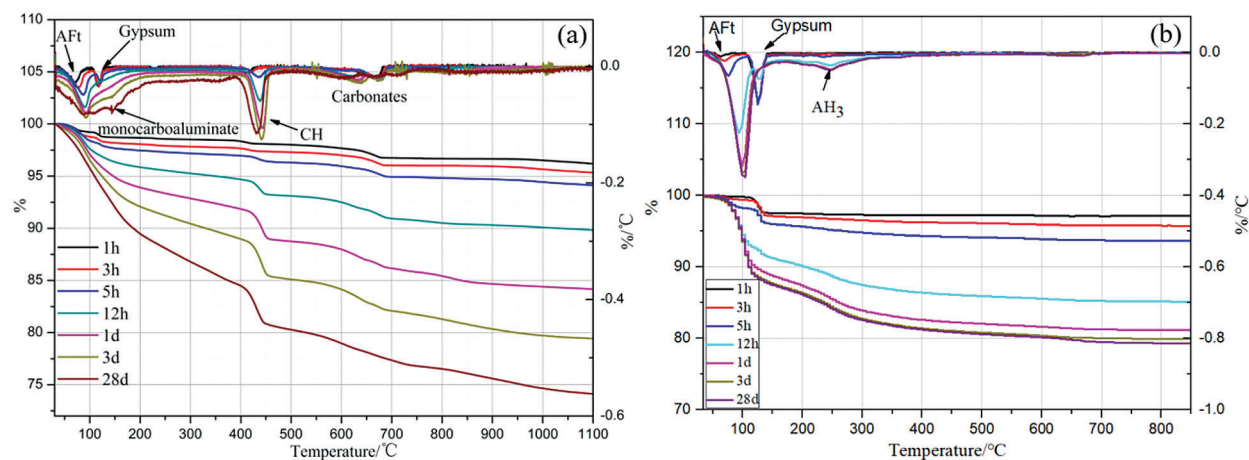


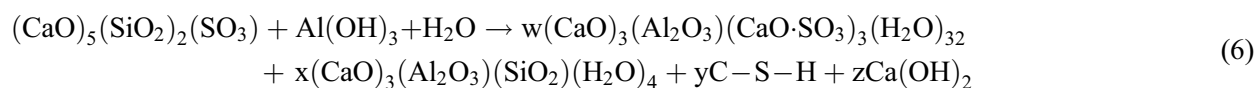
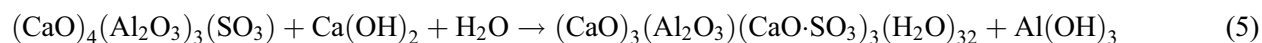
Figure 11: TGA curves of OPC (a) and TY cement (b) hydrates

In TY cement system, the hydration products are mainly ettringite, a small amount of $3\text{CaO}\cdot\text{Al}_2\text{O}_3\cdot\text{SiO}_2\cdot 4\text{H}_2\text{O}$ and C–S–H [41]. AFt began to appear at 1 h and gradually increased from 1 h to 28 d, while ye’elinite and gypsum gradually disappeared. At 12 h, it was found that ye’elinite and gypsum were dramatically consumed. The main reason was that the addition of gypsum promoted the formation of ye’elinite and thus promoted large quantities of ettringite in the early stage. The diffraction peak of ternesite does not change significantly in the early stage and decreases slightly after 28 d of hydration, which indicates that the early compressive strength of the TY cement is mainly provided by the ye’elinite. With the extension of hydration age, ternesite will undergo some hydration reactions. However, no diffraction peaks were observed in the XRD pattern for the gypsum dihydrate produced by the hydration of ternesite, which should be because gypsum continued to participate in hydration to form AFt [9]. In the patterns of TGA, the weight losses from 50 to 110°C, 110–140°C and 200–300°C indicate the loss of AFt, gypsum and aluminum hydroxide gel. The loss of AFt became faster after 12 h. The presence of aluminium hydroxide ($\text{Al}(\text{OH})_3$) was observed, but the diffraction peak was not observed in XRD patterns. Because the $\text{Al}(\text{OH})_3$ is certainly amorphous or micro-crystalline, as it was not observed in any XRD spectrum.

3.2.3 Characterization of the Microstructure of the Hydrates

The hydrated samples of TY cement were analyzed by SEM to determine the mineralogical composition of their hydrated matrix.

In the early stage of hydration, ye’elinite rapidly reacted with gypsum to produce a large amount of AFt (Eq. (5), Fig. 12a) [29,30,33–34]. In the middle of hydration, AFt, C–S–H, (Eq. (6), Fig. 12b), and $\text{Ca}(\text{OH})_2$ were further generated due to the continued reaction between ternesite and ye’elinite hydrated $\text{Al}(\text{OH})_3$ [19–21]. It can be well observed that AFt is generated in large quantities and distributed evenly all over the sample. C–S–H is agglomerated on AFt matrix, and $\text{Ca}(\text{OH})_2$ flake is produced in the AFt gap.



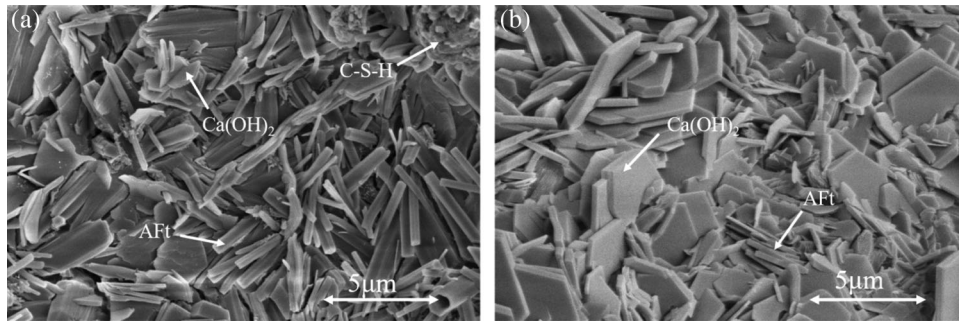


Figure 12: SEM images of hydrates of TY cement at 28 d

3.2.4 Mechanical Strength

The compressive strength comparison between OPC and TY cement clinker is shown in Fig. 13. The compressive strength of TY cement increased rapidly at the early stage, which is much higher than that of OPC. The early compressive strength of TY cement was increased by approximately 4 MPa compared to OPC at 3 d. The increase of the early strength is attributed to the large amount of ettringite produced from rapid reaction of ye'elite and gypsum. At 14 d, the compressive strength of TY cement was increased by approximately 1.5 MPa compared to OPC. The compressive strength of TY cement at 28 d is slightly higher than that of OPC.

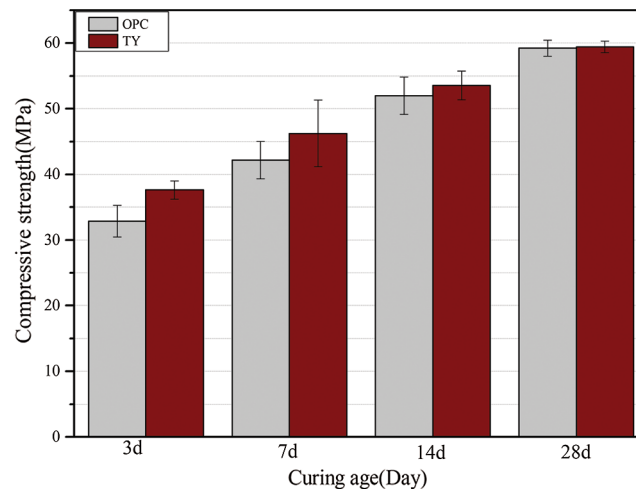


Figure 13: Compressive strength of OPC and TY cement

The mathematical function model of compressive strength of OPC and TY cement is shown in Fig. 14. The relationship between compressive strength (MPa) and curing time (d) of OPC cement satisfies the mathematical model: $y = 0.9912x + 33.673$, R^2 (Fit factor) = 0.8966. And the relationship between compressive strength (MPa) and curing time (d) of TY cement satisfies the mathematical model: $y = 0.8041x + 38.761$, R^2 (Fit factor) = 0.8791.

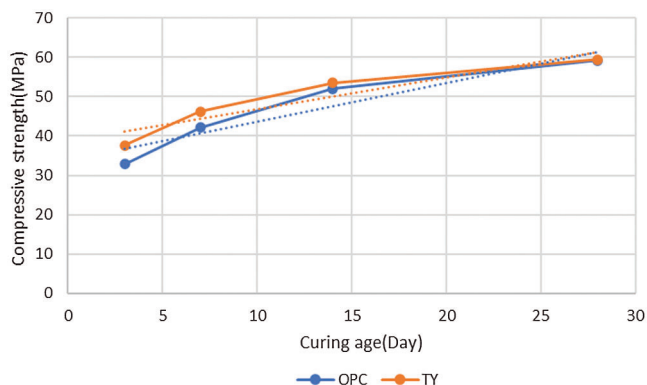


Figure 14: Mathematical function model of compressive strength of OPC and TY cement

4 Conclusion

To summarize, the composition and performance of TY clinker produced from steel slag were investigated in this paper. Ternesite and ye'elimite were produced in large quantities when calcined at 1200°C, which is 100°C lower than the traditional one-step method. The clinker minerals are ternesite, ye'elimite, gypsum and a small amount of iron phase.

Compressive strength of TY increased rapidly in the first and middle stage, but slowly in the later stage. The strength of cement at 28 d is 59.5 MPa that is higher than OPC. Therefore, the steel slag can be directly utilized by this energy-efficient method and the resultant TY clinker possesses a higher performance compared with OPC.

Funding Statement: The authors are grateful for the financial support of the National Natural Science Foundation of China (Grant No. 51872252) and the Postgraduate Research & Practice Innovation Program of Jiangsu Province, China (Grant No. SJCX20 1356).

Conflicts of Interest: The authors declare that they have no conflicts of interest to report regarding the present study.

References

1. Tsakiridis, P. E., Papadimitriou, G. D., Tsvivilis, S., Koroneos, C. (2008). Utilization of steel slag for Portland cement clinker production. *Journal of Hazardous Materials*, 152(2), 805–811. DOI 10.1016/j.jhazmat.2007.07.093.
2. Qiang, W., Yan, P. (2010). Hydration properties of basic oxygen furnace steel slag. *Construction and Building Materials*, 24(7), 1134–1140. DOI 10.1016/j.conbuildmat.2009.12.028.
3. Cao, L., Shen, W., Huang, J., Yang, Y., Zhang, D. et al. (2019). Process to utilize crushed steel slag in cement industry directly: Multi-phased clinker sintering technology. *Journal of Cleaner Production*, 217, 520–529. DOI 10.1016/j.jclepro.2019.01.260.
4. Palankar, N., Shankar, A., Mithun, B. M. (2016). Durability studies on eco-friendly concrete mixes incorporating steel slag as coarse aggregates. *Journal of Cleaner Production*, 129, 437–448. DOI 10.1016/j.jclepro.2016.04.033.
5. Qasrawi, H., Shalabi, F., Asi, I. (2009). Use of low CaO unprocessed steel slag in concrete as fine aggregate. *Construction and Building Materials*, 23(2), 1118–1125. DOI 10.1016/j.conbuildmat.2008.06.003.
6. Kong, Y., Wang, P., Liu, S. (2018). Microwave pre-curing of Portland cement-steel slag powder composite for its hydration properties. *Construction and Building Materials*, 189, 1093–1104. DOI 10.1016/j.conbuildmat.2018.09.088.
7. Iacobescu, R. I., Angelopoulos, G. N., Jones, P. T., Blanpain, B., Pontikes, Y. (2016). Ladle metallurgy stainless steel slag as a raw material in ordinary Portland cement production: A possibility for industrial symbiosis. *Journal of Cleaner Production*, 112(2), 872–881. DOI 10.1016/j.jclepro.2015.06.006.

8. Brotherton, P. D., Epstein, J. M., Pryce, M. W., White, A. H. (1974). Crystal structure of 'calcium sulposilicate', $\text{Ca}_5(\text{SiO}_4)_2\text{SO}_4$. *Australian Journal of Chemistry*, 27(3), 657–660. DOI 10.1071/ch9740657.
9. Shen, Y., Qian, J., Huang, Y., Yang, D. (2015). Synthesis of belite sulfoaluminate-ternesite cements with phosphogypsum. *Cement and Concrete Composites*, 63, 67–75. DOI 10.1016/j.cemconcomp.2015.09.003.
10. Solon, S., Gabriel, J., Isabel, G., Mark, W., Ammar, E. et al. (2018). The synthesis and hydration of ternesite, $\text{Ca}_5(\text{SiO}_4)_2\text{SO}_4$. *Cement and Concrete Research*, 113, 27–40. DOI 10.1016/j.cemconres.2018.06.012.
11. Hanein, T., Galan, I., Glasser, F., Skalamprinos, S., Elhoweris, A. et al. (2017). Stability of ternesite and the production at scale of ternesite-based clinkers. *Cement & Concrete Research*, 98(1), 91–100. DOI 10.1016/j.cemconres.2017.04.010.
12. Irran, E. (1997). Ternesite, $\text{Ca}_5(\text{SiO}_4)_2\text{SO}_4$, a new mineral from the Ettringer Bellerberg/Eifel, Germany. *Mineralogy and Petrology*, 60, 121–132. DOI 10.1007/BF01163138.
13. Bullerjahn, F., Schmitt, D., Haha, M. B. (2014). Effect of raw mix design and of clinkering process on the formation and mineralogical composition of (ternesite) belite calcium sulphoaluminate ferrite clinker. *Cement and Concrete Research*, 59(5), 87–95. DOI 10.1016/j.cemconres.2014.02.004.
14. Powers, M. B., Vedel, E., Emmelkamp, P. (2008). Behavioral couples therapy (BCT) for alcohol and drug use disorders: A meta-analysis. *Clinical Psychology Review*, 28(6), 952–962. DOI 10.1016/j.cpr.2008.02.002.
15. Shen, Y., Chen, X., Zhang, W., Li, X. (2019). Effect of ternesite on the hydration and properties of calcium sulfoaluminate cement. *Journal of Thermal Analysis and Calorimetry*, 136, 687–695. DOI 10.1007/s10973-018-7685-x.
16. Beretka, J., Marroccoli, M., Sherman, N., Valenti, G. L. (1996). The influence of $\text{C}_4\text{A}_3\bar{\text{S}}$ content and WS ratio on the performance of calcium sulfoaluminate-based cements. *Cement and Concrete Research*, 26, 1673–1681. DOI 10.1016/S0008-8846(96)00164-0.
17. Bullerjahn, F., Zajac, M., Haha, M. B. (2015). CSA raw mix design: Effect on clinker formation and reactivity. *Materials and Structures*, 48(12), 3895–3911. DOI 10.1617/s11527-014-0451-z.
18. Sherman, N., Beretka, J., Santoro, L., Valenti, G. L. (1995). Long-term behaviour of hydraulic binders based on calcium sulfoaluminate and calcium sulfoaluminat. *Cement and Concrete Research*, 25(1), 113–126. DOI 10.1016/0008-8846(94)00119-J.
19. Choi, G. S., Glasser, F. P. (1988). The sulphur cycle in cement kilns: Vapour pressures and solid-phase stability of the sulphate phases. *Cement and Concrete Research*, 18(3), 367–374. DOI 10.1016/0008-8846(88)90071-3.
20. Beretka, J., Cioffi, R., Marroccoli, M., Valenti, G. L. (1996). Energy-saving cements obtained from chemical gypsum and other industrial wastes. *Waste Management*, 16(1–3), 231–235. DOI 10.1016/S0956-053X(96)00046-3.
21. Gutt, W. W. (1968). Manufacture of Portland cement from phosphatic raw materials. *Proceedings of the Fifth International Symposium on the Chemistry of Cement*, vol. 1, pp. 93–105. Tokyo.
22. Gilioli, C., Massazza, F., Pezzuoli, M. (1979). Studies on clinker calcium silicates bearing CaF_2 and CaSO_4 . *Cement and Concrete Research*, 9(3), 295–302. DOI 10.1016/0008-8846(79)90121-2.
23. Timashev, W. W. (1980). The kinetics of clinker formation. The structure and composition of clinker and its phases. *7th International Congress on the Chemistry of Cement*, vol. I, pp. 1–3. Paris.
24. Matalkah, F., Xu, L., Wu, W. (2017). Mechanochemical synthesis of one-part alkali aluminosilicate hydraulic cement. *Materials and Structures*, 50(1), 97. DOI 10.1617/s11527-016-0968-4.
25. Huang, Y., Shen, X., Ma, S. (2007). Effect of Fe_2O_3 on the formation of calcium sulphoaluminate mineral. *Journal of the Chinese Ceramic Society*, 35(4), 485–488. DOI 10.1016/S1001-6058(07)60030-4.
26. Hu, Y. (2016). The preparation and composition analysis of alite-ye'elimite with industrial wastes. *Ceramics Silikaty*, 60(3), 1–10. DOI 10.13168/cs.2016.0027.
27. Kurdowski, W., Thiel, A. (1985). Effects of calcium carbide residue and high-silicon limestone on synthesis of belite-barium calcium sulphoaluminate cement. *Journal of Inorganic and Organometallic Polymers and Materials*, 21(4), 900–905. DOI 10.1007/s10904-011-9560-0.
28. Zhang, W., Lu, L., Cui, Y., Chang, J., Cheng, X. (2007). Microstructure and performances of belite-calcium barium sulphoaluminate cement. *Journal of the Chinese Ceramic Society*, 4(1), 77–81.

29. Cline, J. P., Filliben, J. J., Von Dreele, R. B., Winburn, R., Stephens, P. W. (2014). Addressing the amorphous content issue in quantitative phase analysis: The certification of NIST standard reference material 676a. *Acta Crystallographica*, 67(2), 357–367. DOI 10.1107/S0108767311014565.
30. O'Connor, B. H., Raven, M. D. (1988). Application of the Rietveld refinement procedure in assaying powdered mixtures. *Powder Diffraction*, 3(1), 2–6. DOI 10.1017/S0885715600013026.
31. Gallé, C. (2001). Effect of drying on cement-based materials pore structure as identified by mercury intrusion porosimetry: A comparative study between oven-, vacuum-, and freeze-drying. *Cement and Concrete Research*, 31(10), 1467–1477. DOI 10.1016/S0008-8846(01)00594-4.
32. Kumar, R., Bhattacharjee, B. (2003). Study on some factors affecting the results in the use of MIP method in concrete research. *Cement and Concrete Research*, 33(3), 417–424. DOI 10.1016/S0008-8846(02)00974-2.
33. Kumar, A., Roy, D. M. (1985). Diffusion and pore structure in Portland cement pastes blended with low calcium fly ash. *MRS Proceedings*, 65, 227. DOI 10.1557/PROC-65-227.
34. Sahu, S., Tomková, V., Majling, J., Havlica, J. (1993). Influence of particle sizes of individual minerals on the hydration processes in the system $C_2S-C_4A_3S-CS$. *Cement and Concrete Research*, 23(3), 693–699. DOI 10.1016/0008-8846(93)90020-A.
35. Jansen, D., Stabler, C., Goetz-Neunhoeffler, F., Dittrich, S., Neubauer, J. (2011). Does ordinary Portland cement contain amorphous phase? A quantitative study using an external standard method. *Powder Diffraction*, 26(1), 31–38. DOI 10.1154/1.3549186.
36. Cheng, G., Zussman, C. (1963). The crystal structure of anhydrite ($CaSO_4$). *Acta Crystallographica*, 16(8), 767–769. DOI 10.1107/S0365110X63001997.
37. Yamnova, N. A., Zubkova, N. V., Eremin, N. N., Zadov, A. E., Gazeev, V. M. (2011). Crystal structure of larnite $\beta-Ca_2SiO_4$ and specific features of polymorphic transitions in dicalcium orthosilicate. *Crystallography Reports*, 56(2), 210–220. DOI 10.1134/S1063774511020209.
38. Hu, Y., Li, W., Ma, S., Wang, Q., Zou, H. et al. (2018). The composition and performance of alite-ye'elimite clinker produced at 1300°C. *Cement and Concrete Research*, 107(9), 41–48. DOI 10.1016/j.cemconres.2018.02.009.
39. Pedersen, B. F., Semmingsen, D. (1982). Neutron diffraction refinement of the structure of gypsum, $CaSO_4 \cdot 2H_2O$. *Acta Crystallographica*, 38(4), 1074–1077. DOI 10.1107/S0567740882004993.
40. Pöllmann, H. (2017). *Cementitious materials: Composition, properties, application*. Berlin, Germany: De Gruyter. DOI 10.1515/9783110473728-002.
41. Ali, M. M., Gopal, S., Handoo, S. K. (1994). Studies on the formation kinetics of calcium sulphoaluminate. *Cement and Concrete Research*, 24(4), 715–720. DOI 10.1016/0008-8846(94)90196-1.